International Journal of Refractory Metals and Hard Materials 95 (2021) 105464

Contents lists available at ScienceDirect

International Journal of Refractory Metals and Hard Materials

journal homepage: www.elsevier.com/locate/IJRMHM

Ductile to brittle transition temperature of advanced tungsten alloys for nuclear fusion applications deduced by miniaturized three-point bending tests

Chao Yin [a,b,*], Dmitry Terentyev [a], Tao Zhang [c], Shuhei Nogami [d], Steffen Antusch [e], Chih-Cheng Chang [a,b], Roumen H. Petrov [f,g], Thomas Pardoen [b]

[a] *Structural Materials Group, Institute of Nuclear Materials Science, SCK CEN, 2400 Mol, Belgium*
[b] *Institute of Mechanics, Materials and Civil Engineering, UCLouvain, 1348 Louvain-la-Neuve, Belgium*
[c] *School of Physics and Materials Science, Guangzhou University, Guangzhou 510006, China*
[d] *Tohoku University, 6-6-01-2 Aramaki-aza Aoba, Sendai, 980-8579, Japan*
[e] *Karlsruhe Institut für Technologie, Hermann-von-Helmholtz-Platz 1, 76344 Eggenstein-Leopoldshafen, Germany*
[f] *Department of Electrical Energy, Metals, Mechanical Constructions & Systems, Ghent University, 9052 Ghent, Belgium*
[g] *Department of Materials Science and Engineering, Delft University of Technology, Delft 2082, the Netherlands*

ARTICLE INFO

Keywords:
Tungsten
Ductile to brittle transition temperature
Miniaturized three-point bending

ABSTRACT

A large campaign of characterization of the ductile to brittle transition temperature (DBTT) and microstructure has been performed on several commercial and lab-scale pure tungsten grades, potassium doped tungsten alloys, and particle reinforced tungsten grades (with particles of TiC, Y_2O_3, or ZrC), all integrated in a large-scale neutron irradiation campaign. The DBTT is deduced based on miniaturized three-point bending tests to provide reference data for the assessment of the irradiation effects on the tungsten alloys. This miniaturized geometry is designed to minimize the operational cost of neutron irradiation, to speed up post-irradiation examination, and to reduce the amount of nuclear waste. The resulting DBTT ranges from around −15 up to 450 °C, depending on the material. The potassium doped tungsten alloys have the lowest DBTT, followed by rolled ZrC reinforced tungsten grade, commercial pure tungsten grades, lab-scale pure tungsten grades, and other particle reinforced tungsten grades. The crack plane orientation and microstructure with respect to grain shape and grain boundaries significantly affect the DBTT for forged/rolled tungsten products with elongated grains. The L-T orientation has a lower DBTT compared to the T-L orientation. Moreover, the DBTT difference in the L-T and T-L orientation raises with increasing the grain aspect ratio. An attempt is made to establish a relationship between the density of low and high angle grain boundaries and DBTT value. The obtained relationship is discussed in the frame of mechanical processing (i.e., rolling or forging) to optimize the DBTT by optimized manufacturing. The results are compared to recent computational predictions of the DBTT in tungsten.

1. Introduction

Plasma facing components (PFCs) in tokamak nuclear fusion reactors (ITER, DEMO) will be exposed to high heat flux, high energy particles, and fast neutron irradiation. Tungsten, which is well known for its high melting point, low erosion rate, low fuel retention, etc., was selected as the main candidate for PFCs, including first wall armor for blanket and divertor [1–3]. During normal operation of a tokamak, the divertor will undergo periodical heat loads, leading to thermal fatigue, and the generation of permanent deformation and cracks over long-term operation [4]. This is why the mechanical properties of tungsten are essential for its assessment as PFC material. As a matter of fact, tungsten has a relatively high ductile to brittle transition temperature (DBTT) already in the non-irradiated state [5–7], and move up to even higher temperature range after neutron irradiation [8–11].

In order to solve the problem of irradiation embrittlement, the European Fusion research program [12] has conducted a major study about risk mitigation materials with a primary purpose of reducing the DBTT (without significant altering other properties). The other target is to improve the resistance to irradiation damage by engineering a dedicated

* Corresponding author.
E-mail address: cyin@sckcen.be (C. Yin).

https://doi.org/10.1016/j.ijrmhm.2020.105464
Received 9 September 2020; Received in revised form 15 December 2020; Accepted 16 December 2020

microstructure through thermo-mechanical processing (i.e., rolling or forging), alloying, and particle reinforcement [13–17]. In order to validate the currently developed materials, a screening neutron irradiation campaign was recently performed in the Belgian material test reactor (BR2), and the post irradiation examination study is currently ongoing.

There are three main ways described in the literature to reduce the DBTT of BCC metals in general and tungsten in particular: via mechanical (or thermo-mechanical) processing (i.e., rolling or forging) [13], by alloying with Re [18], and/or by refining and strengthening the grain boundaries [16,19]. When tungsten is plastically deformed by rolling or forging, the dislocation density increases leading to a network of low angle grain boundaries (LAGB). Since the plastic deformation in BCC metals is controlled by the movement of dislocations, LAGBs are important structural defects that can be a source of edge or mixed dislocations [20], thereby contributing positively to the ductility below the temperature for the activation of screw dislocation motion. Alternatively, in single crystals or recrystallized polycrystalline tungsten, the DBTT corresponds to the activation of the slip of screw dislocations [21–23]. The alloying of tungsten with Re, as reported by Romaner et al. [18], modifies the core of the $1/2 \langle 111 \rangle$ screw dislocation from a symmetric to an asymmetric structure, which assists the nucleation of kinks on the dislocation line, thereby allowing the dislocation to move at a lower shear stress as well as to emit kinks in different planes. As a result, the ductility of tungsten at low temperature is enhanced since a higher number of slip planes are available, and the critical stress to induce plastic deformation is reduced.

Upon severe mechanical loading in the temperature region close to the DBTT, cracks usually initiates near grain boundaries. A grain boundary is usually the weakest link in (fully dense, defect free) metals in general and in tungsten in particular. One of the most common reasons for this behavior is the segregation of impurities, like oxygen and nitrogen, whose presence reduces the cohesive strength of grain boundaries while suppressing intergranular plastic slip. Thus, at sufficiently low temperatures, tungsten might exhibit an intergranular brittle fracture mode before the applied load reaches the critical stress for plastic deformation to occur. In order to prevent such a failure mode, the overall amount of impurities or the concentration of impurities at grain boundaries should be reduced. The impurities can be removed by introducing secondary particles, which can trap impurities into chemical compounds [16]. The reduction of impurities per unit length of grain boundaries can also be achieved by reducing the grain size (i.e., increasing grain boundary density) [19]. Smaller grains have a larger surface-to-volume ratio, and thus the density of the impurities per grain boundary unit surface unit will be reduced given a fixed concentration of impurities in the material.

Mechanical testing of neutron irradiated samples of standardized dimensions is associated with high cost and complicated logistics driven by the need of usage of hot cells (negatively pressurized chamber protecting operator from the ionizing irradiation emitted by the neutron irradiation samples) equipment. The neutron irradiation itself is very costly due to the large infrastructure required for the operation of material test reactors (MTR). The irradiation volume primarily defines the cost because of usage of neutrons for other competing purposes (e.g., medical isotope production, silicon doping, etc.). Therefore, small size testing techniques (SSTT) [24,25] and surrogate irradiation sources, like high energy proton or heavy ion irradiation, which can generate similar irradiation damage pattern as neutron irradiation, are introduced [26–28]. They cannot substitute neutron irradiation for the qualification of mechanical properties to be accepted by regulatory bodies, but the application of surrogate irradiation can certainly move forward the screening and down selection of the advanced materials compared to the baseline ones (for which the effect of neutron irradiation is already assessed), thereby optimizing (reducing the cost of) the test matrix to be executed on MTRs. Our earlier work presents an example, how the unnotched miniaturized three-point bending test was demonstrated to be capable of deducing the DBTT region in adequate agreement with the results obtained using fracture toughness samples of standardized geometry [29]. Moreover, many other materials research institutes around the world, which focused on fusion applications, have implemented and investigated similar miniaturized three-point bending test methods for tungsten alloys and its composites [16,30–34].

Here, we report an investigation of the mechanical properties of risk-mitigation materials (together with reference commercial W grades) to set-up a reference database for the determination of the mechanical properties after neutron irradiation. The mechanical properties of non-irradiated tungsten grades are studied using miniaturized three-point bending specimens, which are categorized as one of the configurations belonging to the SSTT portfolio. The sample geometry and equipment applied in this study are exactly the same as those implemented for testing neutron irradiated samples in the screening neutron irradiation campaign for the down selection of advanced W-based materials.

2. Experimental details

2.1. Materials

Nine different types of tungsten grades are investigated in this study:

- There are two commercial ITER grades of pure tungsten, which are named IGP and ATW produced by Plansee, Austria, and AT&M, China, respectively. Respectively, IGP and ATW has carrot-like grains and pancake-like grains because of the different processes after powder metallurgy sintering, where IGP is double hammered into a rod with a 35 mm × 35 mm cross section, and ATW is rolled into 13 mm thick plate.
- Another pure tungsten grade is made of a fine grain tungsten (FG) produced by spark plasma sintering (SPS) is provided by the Institute of Plasma Physics, Czech Republic.
- Besides pure tungsten, there are three kinds of potassium doped tungsten alloys with pancake-like grains: potassium doped pure tungsten (ALK), potassium doped tungsten alloyed with 3 wt% of rhenium (ALKR), and heavily deformed potassium doped pure tungsten (HDK). ALK and ALKR products, which are manufactured by A.L.M.T., are rolled into 7 mm sheet [35]. HDK is heavily deformed by rolling into 1 mm sheet, as developed by Karlsruhe Institute of Technology, Germany.
- Finally, three kinds of particle reinforced tungsten alloys are also studied, reinforced with 1 wt% TiC (W1TiC), 2 wt% Y_2O_3 (W2YO), and 0.5 wt% ZrC (W0.5ZrC). W1TiC and W2YO are produced with powder injection molding (PIM) and provided by Karlsruhe Institute of Technology, Germany. Because no rolling or forging is applied in the context of the PIM process, W1TiC and W2YO have equiaxed grains. Institute of Solid State Physics, China provides the W0.5ZrC, which is rolled and treated with thermal mechanical treatment (TMT) in order to get semi-equiaxed grains.

The tungsten grades are categorized according to their manufacturing process or composition into three groups, which are commercial pure tungsten grades (IGP and ATW), advanced grades (HDK, ALK, ALKR, FG), and particle reinforced grades (W1TiC, W2YO, W0.5ZrC). The inverse pole figures of these tungsten grades are shown in Fig. 1 with the indication of longitudinal direction (LD) and transverse direction (TD). Table 1 provides the composition, medium equivalent diameter (D50), 10% equivalent diameter (D10), and 90% equivalent diameter (D90) of the grains, which are defined as the equivalent grain sizes that are larger than 50%, 10%, and 90% of the total grains, respectively.

2.2. Testing methods

The electron back-scatter diffraction (EBSD) analysis is performed

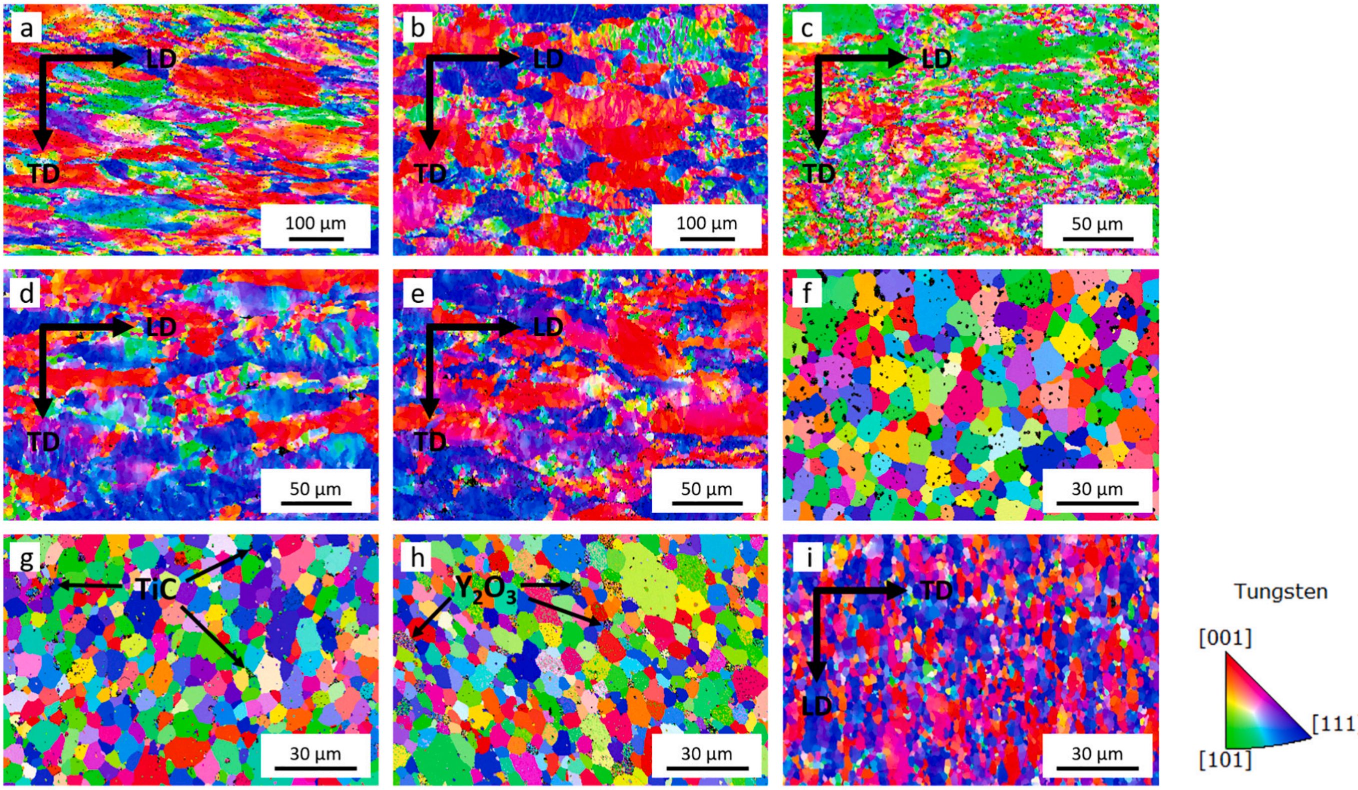

Fig. 1. Inverse pole figure of different tungsten grades: (a) IGP; (b) ATW; (c) HDK; (d) ALK; (e) ALKR; (f) FG; (g) W1TiC; (h) W2YO; (i) W0.5ZrC. The figure for IGP, ATW, FG, W1TiC, W2YO, W0.5ZrC has been reported in our previous work [36].

Table 1
Chemical composition and grain size of different tungsten grades. The compositions of the commercial grades are provided by the manufacturer.

Materials	Major composition (by weight)	D10 (μm)	D50 (μm)	D90 (μm)
IGP	Pure W (>99.97%)	15.74	87.44[36]	151.51
ATW	Pure W (>99.94%)	21.16	60.28[36]	139.73
HDK	Pure W + 60 ppm of K [37]	3.47	26.52	111.05
ALK	Pure W + 30 ppm of K [14]	7.73	37.04	108.92
ALKR	97% W + 3% Re + 28 ppm of K [14]	6.98	32.65	60.77
FG	Pure W (>99.7%) [38]	4.74	9.36[36]	15.64
W1TiC	99% W + 1% TiC [39]	4.06	7.76[36]	12.06
W2YO	98% W + 2% Y_2O_3 [39]	4.09	7.32[36]	11.76
W0.5ZrC	99.5% W + 0.5% ZrC [16]	2.55	6.66[36]	14.15

using an OIM analysis software. The grain boundary analysis is based on the scan with a step size of ~0.54 μm in an area around 270 × 200 μm^2 on the plane normal to ND. LAGB and high angle grain boundaries (HAGB) are defined as the boundaries with a misorientation angle from 2 to 15° and larger than 15°, respectively. The coincidence site lattices (CSL) boundaries are determined by the Brandon's criterion $\Delta\theta_{max} = \theta\Sigma^{-n}$, where $\Delta\theta_{max}$ is the maxium permissible deviation from coincidence, θ is a constant equal to 15°, n is a constant equal to 0.5, and the boundary fraction is from Σ3 to Σ27. The grain boundary density for each type of grain boundary is defined as the total length of each type of boundary per unit area.

Miniaturized bending specimens are tested using the three-point bending configuration, as shown in Fig. 2(a). The specimen with a mirror-like surface (as shown in Fig. 2(b)) is manufactured by electrical discharge machining (EDM) from the supplied block. The length of the specimen is 12 mm, and both of its width and height are 1 mm. As shown in Fig. 2(c), two orientations are investigated in this study: T-L and L-T, as defined in the ASTM standard E399: the long dimensions of the T-L specimen and L-T specimen are parallel to the TD and LD directions, respectively. The three-point bending tests are performed on a universal testing machine equipped with an environmental furnace operated in air atmosphere. The test temperature is measured by a thermocouple located close to the specimen. The measurement range for the applied thermocouple is from −196 °C up to 600 °C. In order to ensure homogeneous distribution of temperature over the entire specimen and its holder, the target temperature for each test is held for at least 20 min before starting the test. Moreover, the load and displacement are measured with a strain gauge based load cell and a position encoder for the actuator, respectively. The test is performed at a constant displacement rate with a cross-head speed of 0.723 mm/min equivalent to the (flexural) strain rate of 10^{-3} s^{-1} along the tension side of the specimen. The design of the test set-up follows the ASTM standard E290 where the three pins for testing have a diameter of 2.5 mm, and the span of the lower pins is equal to 8.5 mm. The scheme of the test set-up with specimen orientation is shown in Fig. 2(d) where the X-direction is TD and Y-direction is LD for T-L specimens, and vice versa for the L-T specimens.

The flexural strain (FS) is determined as,

$$FS = \frac{6Dd}{L^2} \tag{1}$$

where D is the maximum deflection of the specimen, d is the sample thickness, and L is the span of the lower pins.

By performing the tests in the ductile to brittle transition region, the flexural strain increases from zero to above 10% within a relatively narrow temperature interval. Hence, one can deduce the DBTT by fitting the obtained values and setting a threshold for the flexural strain above which the material could be considered as ductile. The fitting method is a modified version of the one used in our previous work [29]. Here, the upper shift of the flexural strain (FS_{top}) is defined as 10%, and the lower base of the flexural strain (FS_{base}) is defined as 0%. Therefore, a flexural

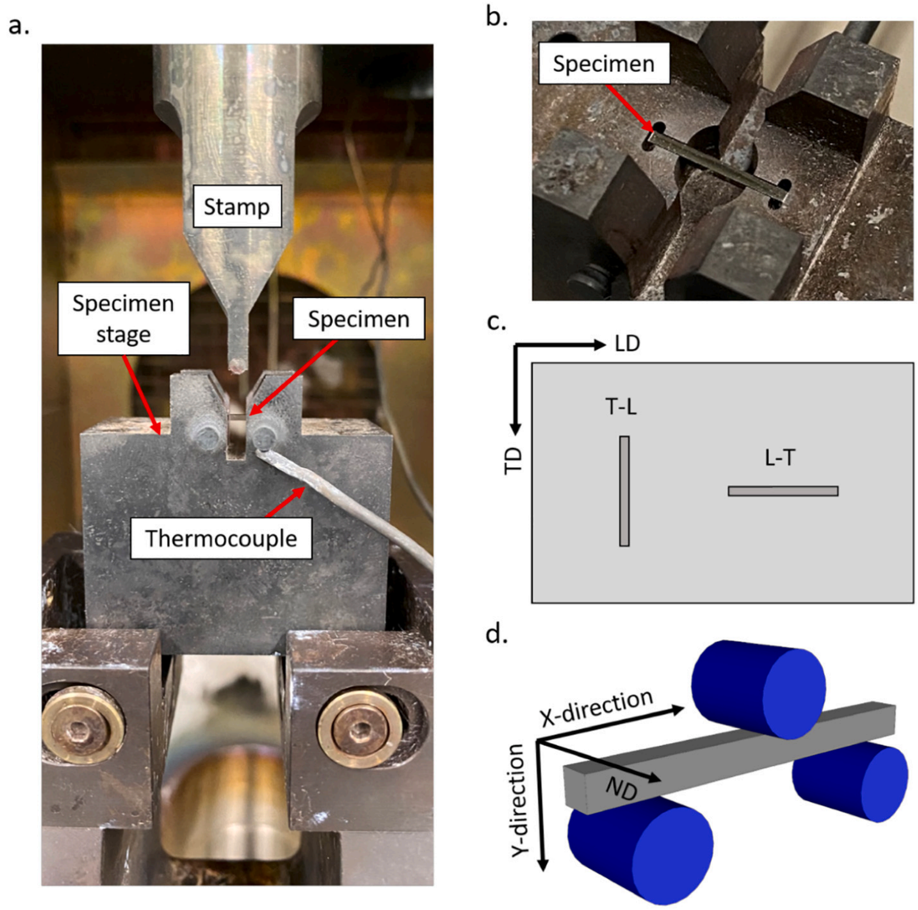

Fig. 2. (a) Three-point bending test configuration; (b) specimen on the test stage; (c) specimen orientation; (d) test set-up of the three-point bending configuration.

strain higher than the defined upper shift will be reported as having a value of 10%. And the equation for fitting the flexural stain transition curve reads as follow:

$$FS(T) = \frac{10\%}{1 + exp\left(C\left(T_{half} - T\right)\right)} \tag{2}$$

where C is the slope of the transition curve; T is the test temperature; T_{half}, which is also defined as the DBTT in this study (following the criterion proposed by [40]), is the temperature corresponding to flexural strain equal to 5%.

3. Results

3.1. Grain boundary density

The grain boundary density and fraction of HAGB, LAGB, and CSL are shown in Fig. 3. The mechanically processed tungsten grades (i.e., IGP, ATW, HDK, ALK, ALKR, and W0.5ZrC) exhibit a much larger density of LAGBs than the grades manufactured by the advanced processes

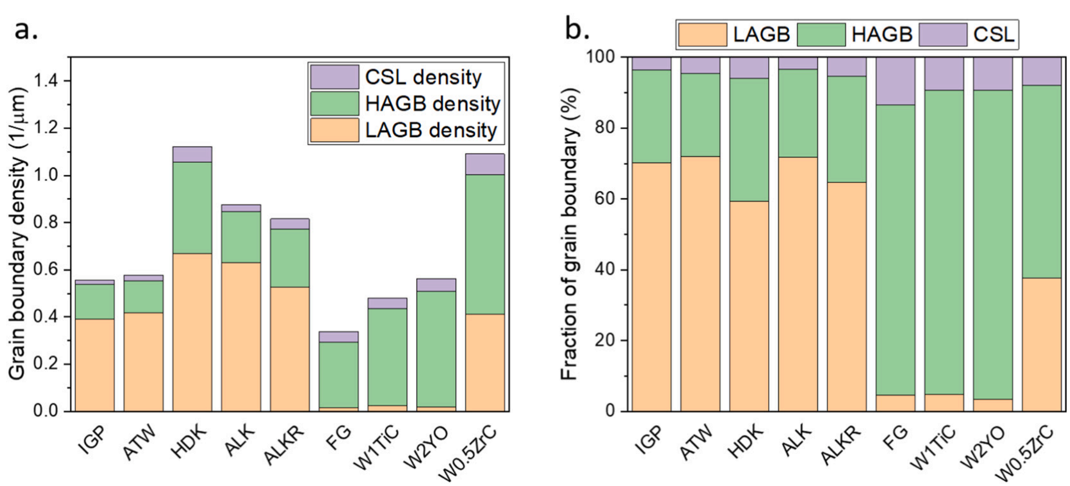

Fig. 3. (a) Grain boundary density and (b) fraction of grain boundary of different tungsten grades.

(i.e., FG, W1TiC, and W2YO). The deformation process during rolling or hammering introduces dislocations and LAGBs (which can be seen as an array of dislocations). The degree of deformation influences the amount of dislocations and LAGBs. As a result, HDK has the highest LAGB density because it is heavily deformed during the manufacturing process. Moreover, with the presence of the potassium bubbles, which will suppress the migration of the grain and dislocation boundaries [37], the removal of LAGB during high temperature mechanical process and heat treatment will be suppressed, which results in a smaller grain size. This can also explain why the HAGB and LAGB density of HDK, ALK, and ALKR are higher than the one of IGP and ATW. The HAGB density of W0.5ZrC, W1TiC, W2YO, and FG are also high since they involve a small grain size, especially for W0.5ZrC, which has the highest HAGB density and the smallest grain size because of the TMT [16]. CSL boundary has a lower boundary energy compared to other HAGBs and is expected to show better resistance to crack propagation (i.e., higher cohesion bonding and lower capacity to suppress plastic slip). Although the absolute CSL density varies in the studied tungsten grades (i.e., W0.5ZrC and HDK have high CSL density), the ratio of CSL boundaries to HAGB fraction is similar for all the tungsten grades, being around 0.11 to 0.15. Given that the fraction of CSL boundaries is very small compared to LAGBs and/or HAGBs, we include CSL boundaries into the population of HAGBs for further discussion.

3.2. Three-point bending tests

Fig. 4 show the variation of flexural strain as a function of temperature and the fitted curves. The fitting parameters are gathered in Table 2. The orientation of the specimens strongly affects the DBTT, with L-T specimen exhibiting lower DBTT than T-L ones, as shown in Fig. 4(a) and (c). Compared to the commercial grades IGP and ATW in Fig. 4(a), the potassium doped tungsten has lower DBTT, especially ALKR L-T, with a DBTT below 0 °C, as shown in Fig. 4(b). The addition of Re is indeed known to enhance the mobility of ½⟨111⟩ screw dislocations (due

Table 2
Fitting parameters for the flexural strain transition curve of various tungsten grades.

Materials	T_{half}	C
IGP L-T	145 ± 1	0.085 ± 0.007
IGP T-L	391 ± 13	0.022 ± 0.006
ATW L-T	220 ± 9	0.050 ± 0.021
ATW T-L	307 ± 6	0.048 ± 0.014
HDK L-T	105 ± 2	0.039 ± 0.002
ALK L-T	65 ± 3	0.048 ± 0.007
ALKR L-T	−14 ± 7	0.051 ± 0.018
FG	304 ± 17,141	0.645 ± 2925.228
W1TiC	394 ± 8	0.012 ± 0.002
W2YO	448 ± 20	0.008 ± 0.002
W0.5ZrC L-T	132 ± 3	0.103 ± 0.025
W0.5ZrC T-L	296 ± 5	0.067 ± 0.020

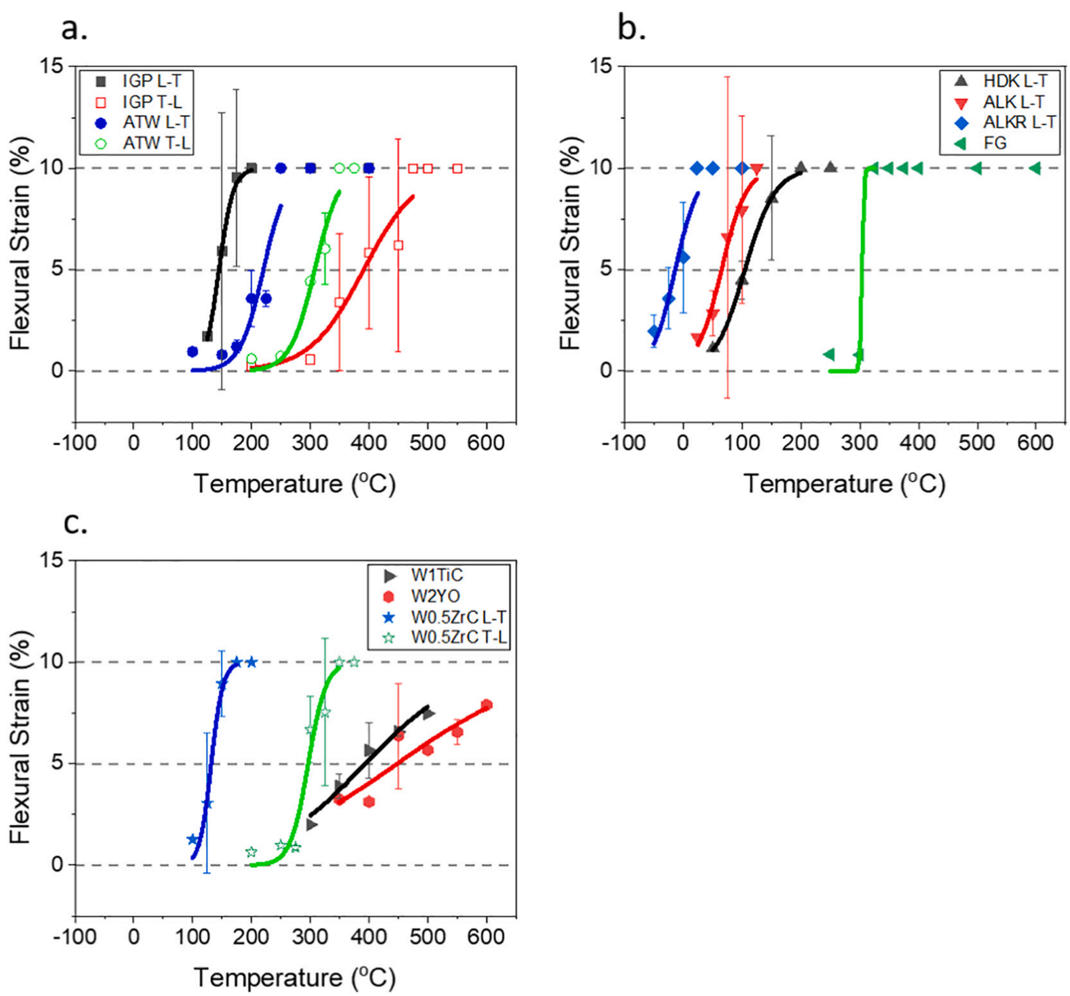

Fig. 4. The flexural strain of different tungsten alloys as a function of temperature. (a) Commercial tungsten grades; (b) Advanced tungsten grades; (c) Particle reinforced tungsten grades. The data of IGP T-L and ATW T-L can be referred to our previous work [29].

to modification of its core structure) and thereby to reduce the DBTT of W—Re alloys [18]. Moreover, the grain size in the potassium doped tungsten grades is smaller than in the commercial pure grades. Smaller grain sizes result in a higher density of dislocation sources, which also contributes to the improvement of low temperature ductility [41,42]. As a result, the toughness and strength of such materials should be higher together with the reduced DBTT compared to tungsten with a larger grain size.

Tungsten grades manufactured without mechanical treatment like rolling or forging have a higher DBTT. Without mechanical treatment, the dislocation density of the material will be lower. As a result, the ductility of tungsten is reduced. Moreover, the temperature span of the transition of W1TiC, W2YO, and FG are different from other tungsten grades, where W1TiC and W2YO have a wider temperature span, and FG shows a very sharp transition. The sharp transition of FG results in missing data points in the transition region and therefore has a very large standard error for the fitting parameters. This sharp transition of FG has also been observed in fracture toughness tests [43].

4. Discussion

4.1. Dependence of DBTT on grain orientation

Early studies conducted by Reiser et al. [44] have shown that for the heavily deformed W plate (HDK, here) the DBTT in the rolling and transversal direction differs by 100 °C. At the same time, Shen et al. [45] reported the difference of DBTT in rolling and transversal direction to be about 50 °C for the commercial rolled W (ATW, here) based on tensile tests, which is in a reasonable agreement with the result obtained here (~100 °C). As was recently studied by Oude Vrielink et al. [46], the dependence of the DBTT on the loading direction can be understood by introducing a cleavage criterion based on the maximum principal stress at grain level (given the grain size distribution and crystallographic texture). However, the modeled DBTT difference between the transversal and rolling direction (predicted based on the crystallography texture and the grain distribution of ATW material from [45]) was found to be only 16 °C, which is much lower compared to the experimental data. The explanation for this difference comes from the fact that different fracture mechanisms (or their mixture) might operate in the different loading directions of rolled/forged tungsten. Moreover, the shape of the elongated grains and their orientation will also influence the DBTT since the anisotropy in the fracture toughness increases with increasing aspect ratio [41]. This is confirmed in Fig. 5 showing that the DBTT difference increases monotonically with the aspect ratio. The IGP has the highest DBTT difference between L-T and T-L orientation, equal

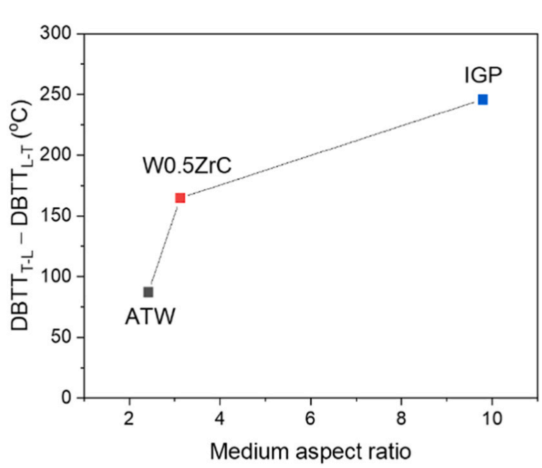

Fig. 5. Anisotropy of DBTT (quantified as the difference of DBTT between T-L and L-T orientation) as a function of medium aspect ratio. The medium aspect ratio of IGP and ATW are taken from [29].

to ~250 °C, and with an aspect ratio of 9.79 [29], followed by W0.5ZrC (DBTT difference of ~160 °C and aspect ratio of 3.12), and finally ATW (DBTT different of ~90 °C and aspect ratio of 2.42 [29]).

The possible explanations for the effect of grain shape on the DBTT are presented in the following. *First*, the correspondence between the main axis of elongated grains and the crack propagation plane are different for T-L and L-T orientations, as shown in Fig. 6(a). For example, the orientation of the elongated grains of IGP T-L samples is along the crack propagation plane. As a result, the crack propagation between elongated grain boundaries will not be deviated/deflected by the grains [29], and this is why IGP has the largest DBTT difference from T-L and L-T orientation. *Second*, since the main free path for dislocation glide varies with the relative angle between the major axis of elongated grains (including subgrains) and the loading direction, the main free path for dislocation glide in grains or subgrains of T-L orientation is shorter than the one of the L-T orientation. Hence, for the T-L orientation, dislocation pile-ups on GBs form at lower values of strain, creating stress concentration and leading to earlier micro-crack nucleation, globally resulting in a lower toughness [41]. Thus, the DBTT of a T-L orientated sample is higher than the L-T. *Third*, the density of grain boundary triple junctions close to the fracture plane of L-T orientation is different from the one of T-L orientation. As presented in Fig. 6(a), section A and section B correspond to the area around the fracture plane for L-T and T-L orientations, respectively. Section A has a larger number of grain boundary triple junctions (indicated as yellow dots) than section B. Upon application of a tensile load to the sample, the stress distributed on each triple junction of the L-T sample is lower than the one of the T-L sample. As a result, the fracture strength (the quotient of load at fracture to the actual fracture cross-section area) of the L-T sample will be higher than the T-L sample. This simple picture is supported by the tensile test results from our earlier studies [11,36], as shown in Fig. 6(b). The fracture strength ($\sigma_{fracture}$) of the tensile sample tested in LD (IGP-L, ATW-L, and W0.5ZrC-L) is regularly higher than the one tested in TD (IGP-T, ATW-T, and W0.5ZrC-T). The fracture plane of LD-loaded and TD-loaded tensile samples is the same as the fracture plane of L-T and T-L bending samples, respectively. The difference of yield strength and ultimate tensile strength for LD and TD loads is small at a test temperature of 600 °C since the plastic deformation at the temperature of 600 °C is mainly governed by the gliding of screw dislocations, and the screw dislocations in tungsten are fully activated at this temperature. Since the yield strength and ultimate tensile strength are almost the same for both L-T and T-L fracture plane, the one with higher $\sigma_{fracture}$, which is the L-T orientation, exhibits lower DBTT.

In order to further validate the hypothesis on the role played by triple junctions, EBSD analysis is performed on a plane normal to LD and TD of IGP, ATW, and W0.5ZrC materials. This approach focuses on HAGB since these interfaces with higher grain boundary energy are more susceptible to crack nucleation and propagation compared to LAGBs. The two sections of Fig. 6(a) can be demonstrated by the grain maps shown in Fig. 7(a), where section A and section B are the plane normal to LD and the plane normal to TD, respectively. The HAGB triple junction density can be estimated as follows. First, the grain shape is approximated by a hexagonal geometry, as shown in Fig. 7(b). The triple junctions (red dots) are located at the six corners of the hexagonal grain, and each triple junction is shared by three grains. Thus, each grain has two triple junctions. Based on this assumption, the number of triple junctions per unit area (D_{tj}) can be estimated by Eq. (3):

$$D_{tj} = \frac{2\left(N_{grain} + \frac{1}{2}N_{edge\ grain}\right)}{A_{scan}}, \tag{3}$$

where N_{grain} is the number of grains, which does not contact the edge of the grain map, $N_{edge\ grain}$ is the number of grains, which contacts the edge of the grain map, and A_{scan} is the area of the IPF map. The relationship between D_{tj} and the orientation dependence of the DBTT and of $\sigma_{fracture}$ is

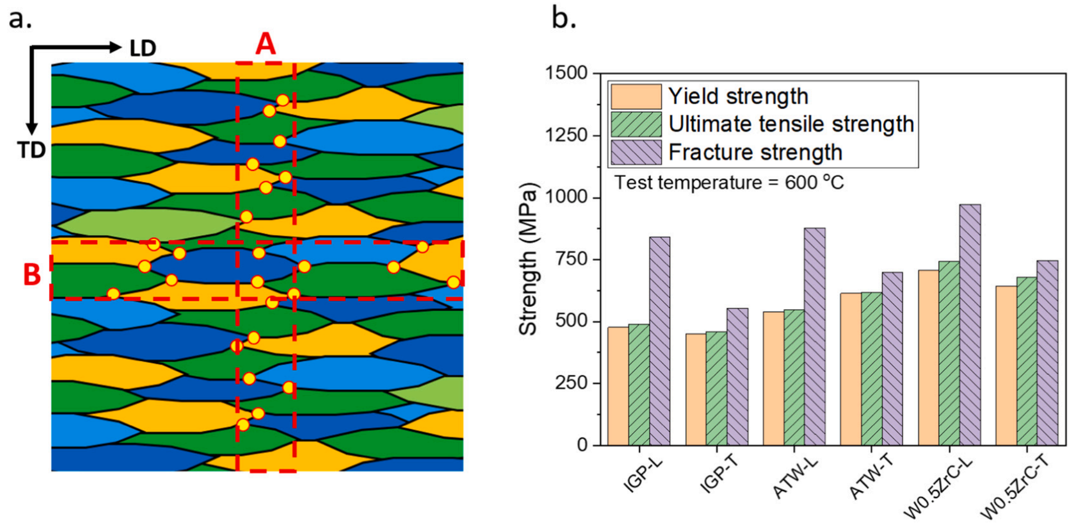

Fig. 6. (a) Grain boundary triple junctions of tungsten with elongated grains; (b) Yield strength, Ultimate tensile strength, and fracture strength of the tensile sample made of IGP, ATW, and W0.5ZrC tested along LD and TD orientation [11,36].

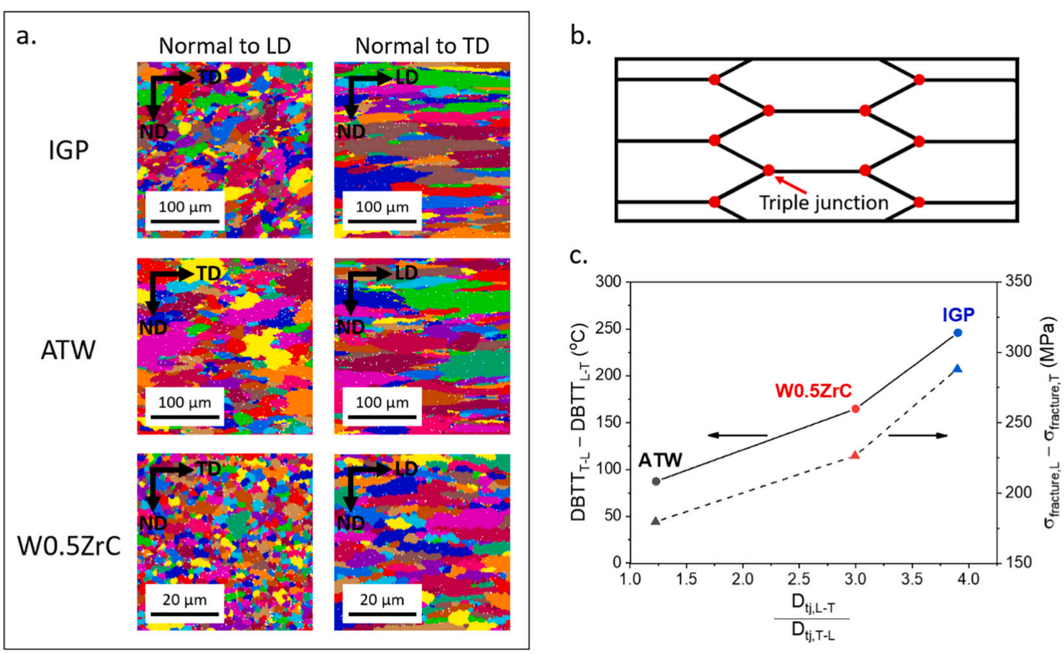

Fig. 7. (a) Grain maps (defined by HAGB) of the plane normal to LD and TD of IGP, ATW, and W0.5ZrC; (b) Hexagonal grains and triple junction points; (c) effect of the triple junction on the DBTT and on $\sigma_{fracture}$ orientation dependence.

shown in Fig. 7(c). The difference of DBTT and $\sigma_{fracture}$ measured for L-T (or L) and T-L (or T) orientation increases with an increasing triple junction density ratio (i.e., $D_{tj,\ L-T}/D_{tj,\ T-L}$). This dependence indicates that the number of grain boundary triple junctions is one of the factors responsible for the orientation dependence of DBTT and $\sigma_{fracture}$, where the orientation with higher D_{tj} in a given tungsten grade results in higher $\sigma_{fracture}$ and lower DBTT.

Another important assumption utilized in the model of Oude Vrielink et al. [46] is that the evolution of plastic deformation (i.e., strain to fracture) is mainly driven by the activation of screw dislocations, which might not necessarily be true in the case of heavily deformed material, where a high density of LAGBs with mixed dislocations is present. The activation of the plastic slip by mixed and edge dislocations stored in the LAGB may also contribute to the macroscopic plastic deformation, and therefore the criterion for the DBTT can be fulfilled below the temperature of the screw dislocation activation.

4.2. DBTT and grain boundary density

Fig. 8(a) shows that the relationship between DBTT and total grain boundary density, which is the sum of CSL density, HAGB density, and LAGB density, has a clear trend. The trend shows that the DBTT reduces with increasing total grain boundary density. Besides the effect of alloying elements and strengthening particles, this phenomenon can be related to an increase of dislocation sources with grain size reduction [41,42]. Moreover, a higher total grain boundary density can reduce the density/size of the clusters of impurities segregating to grain boundaries, thereby preserving the strength of the grain boundaries [19].

In order to analyze the individual contribution of LAGB and HAGB to the DBTT reduction, the DBTT versus LAGB density and versus total

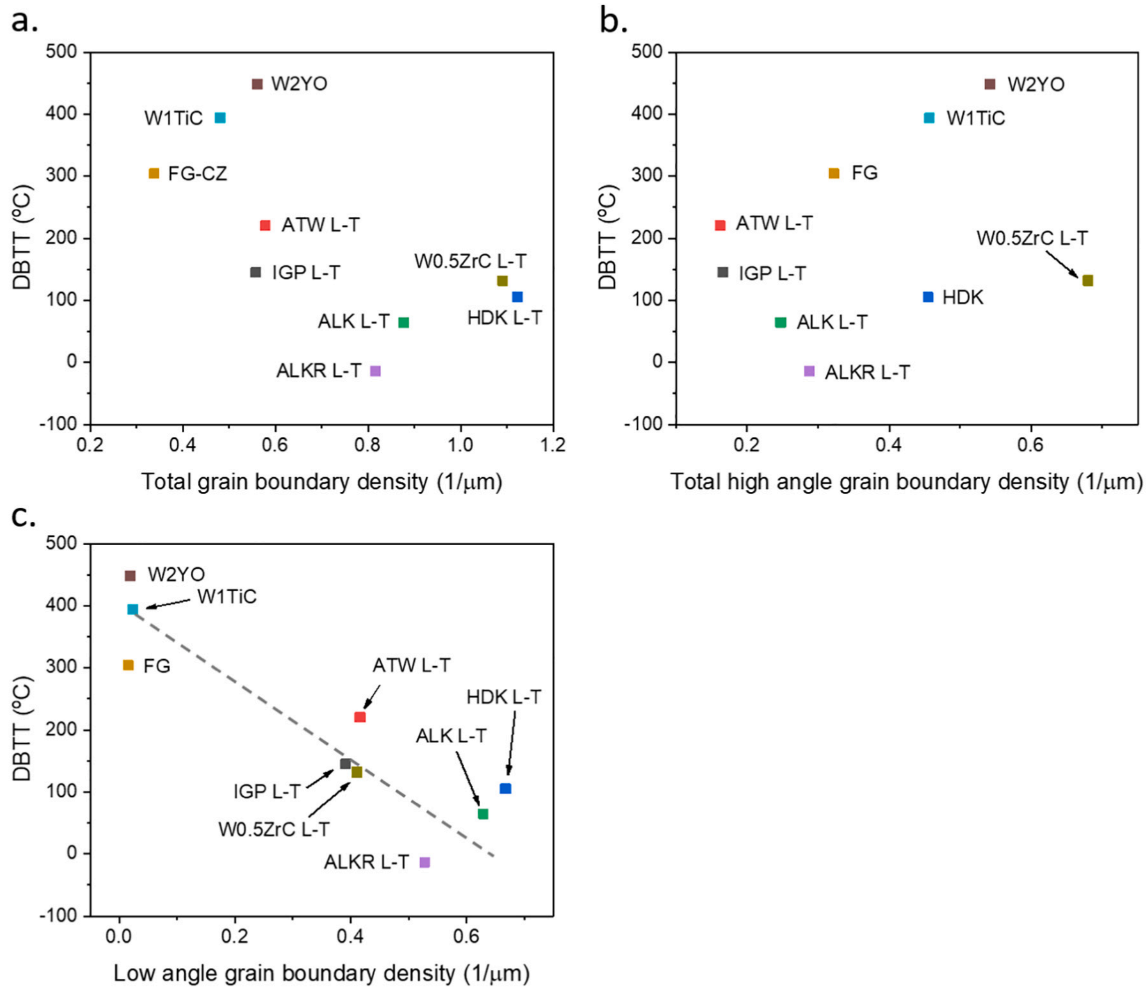

Fig. 8. Relationship between DBTT and grain boundary density. (a) DBTT vs. total grain boundary; (b) DBTT vs. total HAGB; (c) DBTT vs. LAGB.

HAGB density (the sum of CSL and HAGB density) is plotted in two separate figures. Although the relationship between DBTT and total HAGB density, see Fig. 8(b), does not reveal a clear trend, the DBTT has an evident linear reciprocal relationship with the LAGB density as shown in Fig. 8(c). As summarized by Bonnekoh et al. [13], LAGBs can act as dislocation source and thus reduce the DBTT. Moreover, the triple junctions of the LAGBs or HAGBs can act as a source of stress-concentration and crack nucleation. Although the material with high LAGB and HAGB density will have a larger number of stress-concentration sources, the average stress per source is reduced. As a result, the failure of the material is delayed to higher level strains and stresses, which means that the material has a higher toughness. The LAGBs are introduced by mechanical processes like rolling or forging. Therefore, the mechanically processed tungsten grades like potassium doped tungsten grades, commercial tungsten grades, and W0.5ZrC have lower DBTT than FG, W1TiC, and W2YO, which are produced by advanced manufacturing processes.

Although the DBTT shows a strong dependence on the LAGB density, further theoretical and experimental investigation of the role played by LAGBs in the overall process of the macroscopic deformation of polycrystalline tungsten is required. At least two mechanisms of plastic deformation are to be addressed: (i) accumulation of dislocation pile-ups in front of LAGBs and transmission of the dislocations through the LAGBs interfaces; and (ii) conservative grain boundary slip by displacement of the misfit dislocations available at LAGBs. The theoretical and atomistic studies that exist up to day for BCC and FCC metals [47–50] point clearly to the fact that the dissolution of the dislocation pile-ups is thermally activated process which strongly depends on the character of the grain boundary pinning the pile-up. In addition, very recent atomistic simulations indicate that segregation of chemical elements also impact the interaction mechanism [51]. However, in general, one may conclude that the pinning due to HAGBs is expected to be stronger because the transmission requires accumulation of dislocations to enable the emission of the dislocation in a neighboring grain [20]. Whereas, for LAGBs, the interaction with pile-ups boils down to the dislocation-dislocation zip-unzip interaction, which is similar to the bulk dislocation multiplication process [20]. Unfortunately, no such modelling studies are available for tungsten. Clarification of the role played by the dislocation-grain boundary interaction in tungsten will certainly help to understand the role of initial dislocation density on the DBTT and in general on work hardening response of the material. In our recent work, transmission electron microcopy (TEM) was applied to investigate the initial and as-deformed (at 600 °C) microstructure of several tungsten alloys [52], some of which include those studied here. Based on the reported bulk dislocation density [52], one may conclude that the higher the initial dislocation density the lower the DBTT. The microstructure after the deformation at 600 °C indicates that both HAGBs and LAGBs acted as pinning obstacles as well as sources of new dislocation generation. Further TEM information on microstructure upon deformation just above the DBTT is needed to reconcile the role of LAGBs in the plastic deformation process.

4.3. Pros and cons of miniaturized three-point bending tests

Prior to summarize the conclusions, the advantages and caveats of the sub-miniaturized 3 PB testing techniques are discussed. Since the geometry of the miniaturized three-point bending specimen is not complicated to machine, small in volume (i.e. factor 27 volume gain compared to the conventionally accepted KLST sample [53]), and rectangular in shape, it is very efficient to be used for so called “piggy-back” irradiation, when the sample load unit has limited space available. Given the limited dimensions of the sample, the gradient of the heat release and transmutation reactions (materials like tungsten can impose self-shielding effect such that transmutation at the edge of the sample is higher than in its center) under high flux neutron irradiation is also limited compared to standardized samples. Finally, a major advantage of the application of sub-miniaturized samples is their immediate readiness for microstructural or chemical studies after destructive mechanical testing. The application of scanning electron microscopy, focus ion beam milling, or thermal desorption spectroscopy usually is performed in glove boxed (rarely instruments are placed in hot cells) where the ALARA (as low as possible activation) principle defines the permission on usage of the sample, and typically the maximum dose rate on sample contact is limited to 2–5 μSv/h. In the case of the samples studied in this work, half broken 3 PB samples would have a dose rate below 2 μSv/h after receiving about 1 dpa in fission spectrum reactors (like BR2, HFIR, HFR). Hence, the samples can be immediately passed to advanced post-irradiation examination (PIE) without any extra processing. Naturally, the nuclear waste produced by the test campaign utilizing sub-miniaturized samples is essentially reduced.

Besides the above listed advantages, the concern about the representation of the mechanical properties by the miniaturized 3 PB samples compared to standardized samples should not be ignored. Indeed, in the case of sub-miniaturized samples only a small volume of the material undergoes large tensile stress and strain, which is not uniform, in addition. Given that the loaded volume is limited, a special attention needs to be paid to the sample surface preparation. The statistics of the measurements will depend on the surface roughness (the smoother – the better) and if the irradiation experiment does not allow to preserve the original surface roughness (e.g., irradiation in corrosive environment) the eventual post irradiation testing may generate invalid results. The extraction of engineering properties such as yield stress, work hardening rate, and ultimate tensile stress requires rigorous post-processing using finite element method. The validation of such procedures (i.e., extracting true stress – true strain by matching FEM with experimental load – displacement curves) requires additional tests involving tensile samples in reference and equivalent neutron irradiated state. This work is currently ongoing in support of SSTT preparation for DONES-IFMIF [54]. However, given the limited volume in which the accumulation of stress/strain is established, one may also consider the application of surrogate irradiation sources like heavy ion irradiation to damage the region mostly exposed to the tensile deformation. The application of high energy protons (exceeding several MeV) would generate the uniform damage across a thickness of ~1 mm, hence enabling to perform fully valid mechanical testing.

To sum up, the main drawbacks of the sub-miniaturized 3 PB testing are: high precision required for sample preparation and surface roughness, lack of standardized procedure to extract major tensile properties, relatively high number of samples required to establish statistically significant result.

The main advantages are: high efficiency for occupation of the irradiation volume, simple handling for tests in hot cells, immediate (or short-term cooling time) readiness for advanced PIE; low waste.

5. Summary and conclusions

A parametric set of miniaturized three-point bending mechanical tests is performed on various tungsten grades (in non-irradiated state) selected for the screening of their resistance to the neutron irradiation. The final goal beyond this research is to validate the improvement of these tungsten grades regarding the resistance to irradiation degradation. The DBTT is determined based on the flexural bending strain criterion as applied earlier in [29,40], which was proven to be adequate when compared to conventional fracture toughness test methods. SEM-EBSD technique is applied to support a detailed grain boundary structural analysis in order to understand and establish a relationship between the obtained DBTT and grain boundary distribution and morphology. The deduced DBTT values of the different tungsten grades are summarized in Fig. 9. Overall, the DBTT varies from −25 °C up to +450 °C, depending on the grade. The hot rolled W-3%Re material in L-T orientation has the lowest DBTT of −25 °C, which is tentatively explained by synergistic effect of a high density of low angle grain boundaries and addition of Re in solid solution. *Re*-free hot rolled and heavily deformed K-doped tungsten products have the DBTT below 100 °C. The main findings can be summarized as follows:

- For the textured materials, the DBTT is orientation dependent, where L-T orientation has a lower DBTT than T-L for the forged or rolled tungsten grades. The DBTT difference between the L-T and T-L orientations is ranging from ~90 to ~250 °C, which depends on the grain aspect ratio of the tungsten grades. The orientation dependence of the onset of plastic deformation might have strong implications after neutron irradiation during the tokamak operation, as the grains with T-L orientation will be subject to primary loading due to the plasma heat exposure.
- The presence of LAGB has a strong effect on the reduction of the DBTT. For all grades, the DBTT exhibits a linear reciprocal relationship with the LAGB density. The availability of LAGB favors plastic deformation i.e., activation of the edge and mixed dislocations located at the LAGB interfaces, which enables the plastic deformation at temperatures below the one required to activate screw dislocations. On the other hand, the presence of a high density of LAGBs naturally reduces the spacing between grain boundary triple junctions, which are generally considered as sources for stress-concentration and crack nucleation. Correspondingly, the accumulation of the stress concentration at which micro cracks begin to nucleate and then proceed to coalesce is delayed, effectively resulting in the higher fracture stress.
- The mechanical (or even thermo-mechanical) processing during the manufacture (and post fabrication stress-relief) is critical for producing a material with high strength and high ductility simultaneously. Given the relationship between DBTT and the availability of LAGBs, as shown here, an important step for reducing the DBTT is by rolling or forging, which could be enhanced by Re alloying. Particle reinforcement does not have such a strong positive effect on the DBTT reduction. Coupling the particle reinforcement and thermo-mechanical treatment (e.g., W-0.5ZrC) provides a considerable

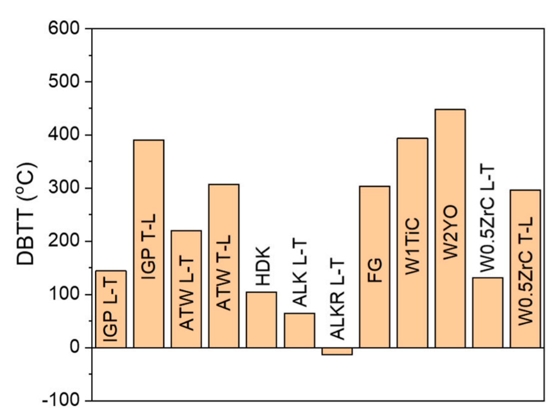

Fig. 9. DBTT of different tungsten grades.

reduction of DBTT (down to ~150 °C) and resistance to high temperature recrystallization. The PIM processing (with or without strengthening particles), which does not involve any rolling or forging, leads to a relatively high DBTT even though the grain size is rather small. The high DBTT of these materials could be explained by the lack of sources for low-temperature plastic deformation.

Declaration of Competing Interest

The authors declare that they have no known competing financial interests or personal relationships that could have appeared to influence the work reported in this paper.

Acknowledgments

This work has been carried out within the framework of the EUROfusion Consortium and has received funding from the Euratom research and training programme 2014-2018 and 2019-2020 under grant agreement No 633053. The views and opinions expressed herein do not necessarily reflect those of the ITER Organization or of the European Commission.

References

[1] R. Pitts, X. Bonnin, F. Escourbiac, H. Frerichs, J. Gunn, T. Hirai, A. Kukushkin, E. Kaveeva, M. Miller, D. Moulton, Physics basis for the first ITER tungsten divertor, Nucl. Mater. Energy 20 (2019) 1–25.
[2] J. You, E. Visca, T. Barrett, B. Böswirth, F. Crescenzi, F. Domptail, M. Fursdon, F. Gallay, B. Ghidersa, H. Greuner, European divertor target concepts for DEMO: design rationales and high heat flux performance, Nucl. Mater. Energy 16 (2018) 1–11.
[3] T.R. Barrett, G. Ellwood, G. Pérez, M. Kovari, M. Fursdon, F. Domptail, S. Kirk, S. McIntosh, S. Roberts, S. Zheng, Progress in the engineering design and assessment of the European DEMO first wall and divertor plasma facing components, Fusion Eng. Des. 109-111 (2016) 917–924.
[4] J. Linke, J. Du, T. Loewenhoff, G. Pintsuk, B. Spilker, I. Steudel, M. Wirtz, Challenges for plasma-facing components in nuclear fusion, Matter Radiat. Extrem. 4 (5) (2019), 056201.
[5] H. Sheng, G. Van Oost, E. Zhurkin, D. Terentyev, V.I. Dubinko, I. Uytdenhouwen, J. Vleugels, High temperature strain hardening behavior in double forged and potassium doped tungsten, J. Nucl. Mater. 444 (1–3) (2014) 214–219.
[6] A. Giannattasio, Z. Yao, E. Tarleton, S.G. Roberts, Brittle-ductile transitions in polycrystalline tungsten, Philos. Mag. 90 (30) (2010) 3947–3959.
[7] D. Rupp, S.M. Weygand, Anisotropic fracture behaviour and brittle-to-ductile transition of polycrystalline tungsten, Philos. Mag. 90 (30) (2010) 4055–4069.
[8] J.M. Steichen, Tensile properties of neutron-irradiated TZM and tungsten, J. Nucl. Mater. 60 (1) (1976) 13–19.
[9] I. Alexandrov, I.V. Gorynin, Metallovedenie 22 (1979) 35.
[10] I.V. Gorynin, V.A. Ignatov, V. Rybin, S.A. Fabritsiev, V.A. Kazakov, V.P. Chakin, V. A. Tsykanov, V.R. Barabash, Y.G. Prokofyev, Effects of neutron-irradiation on properties of refractory-metals, J. Nucl. Mater. 191 (1992) 421–425.
[11] C. Yin, D. Terentyev, T. Zhang, R.H. Petrov, T. Pardoen, Impact of neutron irradiation on the strength and ductility of pure and ZrC reinforced tungsten grades, J. Nucl. Mater. 537 (2020), 152226.
[12] G. Pintsuk, E. Diegele, S.L. Dudarev, M. Gorley, J. Henry, J. Reiser, M. Rieth, European materials development: results and perspective, Fusion Eng. Des. 146 (2019) 1300–1307.
[13] C. Bonnekoh, A. Hoffmann, J. Reiser, The brittle-to-ductile transition in cold rolled tungsten: on the decrease of the brittle-to-ductile transition by 600 K to− 65 C, Int. J. Refract. Met. Hard Mater. 71 (2018) 181–189.
[14] M. Fukuda, S. Nogami, K. Yabuuchi, A. Hasegawa, T. Muroga, Anisotropy in the mechanical properties of potassium and rhenium doped tungsten alloy plates for fusion reactor applications, Fusion Sci. Technol. 68 (3) (2015) 690–693.
[15] M. Fukuda, A. Hasegawa, T. Tanno, S. Nogami, H. Kurishita, Property change of advanced tungsten alloys due to neutron irradiation, J. Nucl. Mater. 442 (1–3) (2013) S273–S276.
[16] Z.M. Xie, R. Liu, S. Miao, X.D. Yang, T. Zhang, X.P. Wang, Q.F. Fang, C.S. Liu, G. N. Luo, Y.Y. Lian, X. Liu, Extraordinary high ductility/strength of the interface designed bulk W-ZrC alloy plate at relatively low temperature, Sci. Rep. 5 (2015) 1–11.
[17] T. Zhang, H. Deng, Z. Xie, R. Liu, J. Yang, C. Liu, X. Wang, Q. Fang, Y. Xiong, Recent progresses on designing and manufacturing of bulk refractory alloys with high performances based on controlling interfaces, J. Mater. Sci. Technol. 52 (2020) 29–62.
[18] L. Romaner, C. Ambrosch-Draxl, R. Pippan, Effect of rhenium on the dislocation core structure in tungsten, Phys. Rev. Lett. 104 (19) (2010) 195503.
[19] Q. Wei, H. Zhang, B. Schuster, K. Ramesh, R. Valiev, L. Kecskes, R. Dowding, L. Magness, K. Cho, Microstructure and mechanical properties of super-strong nanocrystalline tungsten processed by high-pressure torsion, Acta Mater. 54 (15) (2006) 4079–4089.
[20] D. Hull, D.J. Bacon, Introduction to Dislocations, Butterworth-Heinemann, Oxford, 2001.
[21] P. Gumbsch, J. Riedle, A. Hartmaier, H.F. Fischmeister, Controlling factors for the brittle-to-ductile transition in tungsten single crystals, Science 282 (5392) (1998) 1293–1295.
[22] D. Terentyev, X. Xiao, A. Dubinko, A. Bakaeva, H. Duan, Dislocation-mediated strain hardening in tungsten: thermo-mechanical plasticity theory and experimental validation, J. Mech. Phys. Solids 85 (2015) 1–15.
[23] D. Terentyev, X. Xiao, S. Lemeshko, U. Hangen, E.E. Zhurkin, High temperature nanoindentation of tungsten: modelling and experimental validation, Int. J. Refract. Met. Hard Mater. 105222 (2020).
[24] B.J. Kim, R. Kasada, A. Kimura, H. Tanigawa, Evaluation of grain boundary embrittlement of phosphorus added F82H steel by SSTT, J. Nucl. Mater. 421 (1–3) (2012) 153–159.
[25] N. Igata, K. Miyahara, C. Tada, D. Blasl, G. Lucas, Phenomenological studies of the effects of miniaturization and irradiation on the mechanical-properties of stainless-steels, Radiat. Eff. Def. Solids 101 (1–4) (1987) 131–146.
[26] F. F, Y. X, K. Arakawa, S.P. Fitzgerald, P.D. Edmonds, S.G. Roberts, High temperature annealing of ion irradiated tungsten, Acta Mater. 90 (2015) 380–393.
[27] J. Gibson, D. Armstrong, S. Roberts, The micro-mechanical properties of ion irradiated tungsten, Phys. Scripta T159 (2014).
[28] D.E.J. Armstrong, X. Yi, E.A. Marquis, S.G. Roberts, Hardening of self ion implanted tungsten and tungsten 5-wt% rhenium, J. Nucl. Mater. 432 (1–3) (2013) 428–436.
[29] C. Yin, D. Terentyev, T. Pardoen, R. Petrov, Z. Tong, Ductile to brittle transition in ITER specification tungsten assessed by combined fracture toughness and bending tests analysis, Mater. Sci. Eng. A 750 (2019) 20–30.
[30] D. Blagoeva, J. Opschoor, J. Van der Laan, C. Sârbu, G. Pintsuk, M. Jong, T. Bakker, P. Ten Pierick, H. Nolles, Development of tungsten and tungsten alloys for DEMO divertor applications via MIM technology, J. Nucl. Mater. 442 (1–3) (2013) S198–S203.
[31] Z. Zhou, Y. Ma, J. Du, J. Linke, Fabrication and characterization of ultra-fine grained tungsten by resistance sintering under ultra-high pressure, Mater. Sci. Eng. A 505 (1–2) (2009) 131–135.
[32] P. López-Ruiz, N. Ordás, I. Iturriza, M. Walter, E. Gaganidze, S. Lindig, F. Koch, C. García-Rosales, Powder metallurgical processing of self-passivating tungsten alloys for fusion first wall application, J. Nucl. Mater. 442 (1–3) (2013) S219–S224.
[33] B. Jasper, J.W. Coenen, J. Riesch, T. Höschen, M. Bram, C. Linsmeier, Powder metallurgical tungsten fiber-reinforced tungsten, in: Materials Science Forum, Trans Tech Publ, 2015, pp. 125–133.
[34] Y. Ueda, H. Lee, N. Ohno, S. Kajita, A. Kimura, R. Kasada, T. Nagasaka, Y. Hatano, A. Hasegawa, H. Kurishita, Recent progress of tungsten R&D for fusion application in Japan, Phys. Scr. 2011 (T145) (2011), 014029.
[35] S. Nogami, A. Hasegawa, M. Fukuda, S. Watanabe, J. Reiser, M. Rieth, Tungsten modified by potassium doping and rhenium addition for fusion reactor applications, Fusion Eng. Des. 152 (2020) 111445.
[36] C. Yin, D. Terentyev, T. Pardoen, A. Bakaeva, R. Petrov, S. Antusch, M. Rieth, M. Vilemova, J. Matejicek, T. Zhang, Tensile properties of baseline and advanced tungsten grades for fusion applications, Int. J. Refract. Met. Hard Mater. 75 (2018) 153–162.
[37] P. Lied, C. Bonnekoh, W. Pantleon, M. Stricker, A. Hoffmann, J. Reiser, Comparison of K-doped and pure cold-rolled tungsten sheets: as-rolled condition and recrystallization behaviour after isochronal annealing at different temperatures, Int. J. Refract. Met. Hard Mater. 85 (2019) 105047.
[38] L. Tanure, A. Bakaeva, L. Lapeire, D. Terentyev, M. Vilémová, J. Matějíček, K. Verbeken, Nano-hardness, EBSD analysis and mechanical behavior of ultra-fine grain tungsten for fusion applications as plasma facing material, Surf. Coat. Technol. 355 (2018) 252–258.
[39] S. Antusch, D.E.J. Armstrong, T.B. Britton, L. Commin, J.S.-L. Gibson, H. Greuner, J. Hoffmann, W. Knabl, G. Pintsuk, M. Rieth, Mechanical and microstructural investigations of tungsten and doped tungsten materials produced via powder injection molding, Nucl. Mater. Energy 3 (2015) 22–31.
[40] D.H. Lassila, F. Magness, D. Freeman, Ductile-Brittle Transition Temperature Testing of Tungsten Using the Three-Point Bend Test, Report Lawrence Livermore National Laboratory UCRL-ID-108258, 1991.
[41] J. Reiser, A. Hartmaier, Elucidating the dual role of grain boundaries as dislocation sources and obstacles and its impact on toughness and brittle-to-ductile transition, Sci. Rep. 10 (1) (2020) 1–18.
[42] C. Bonnekoh, U. Jäntsch, J. Hoffmann, H. Leiste, A. Hartmaier, D. Weygand, A. Hoffmann, J. Reiser, The brittle-to-ductile transition in cold rolled tungsten plates: impact of crystallographic texture, grain size and dislocation density on the transition temperature, Int. J. Refract. Met. Hard Mater. 78 (2019) 146–163.
[43] D. Terentyev, M. Vilémová, C. Yin, J. Veverka, A. Dubinko, J. Matějíček, Assessment of mechanical properties of SPS-produced tungsten including effect of neutron irradiation, Int. J. Refract. Met. Hard Mater. 89 (2020) 105207.
[44] J. Reiser, S. Wurster, J. Hoffmann, S. Bonk, C. Bonnekoh, D. Kiener, R. Pippan, A. Hoffmann, M. Rieth, Ductilisation of tungsten (W) through cold-rolling: R-curve behaviour, Int. J. Refract. Metals Hard Mater. 58 (2016) 22–33.
[45] T.L. Shen, Y. Dai, Y. Lee, Microstructure and tensile properties of tungsten at elevated temperatures, J. Nucl. Mater. 468 (2016) 348–354.
[46] M.O. Vrielink, J. van Dommelen, M.G. Geers, Numerical investigation of the brittle-to-ductile transition temperature of rolled high-purity tungsten, Mechan. Mater. 145 (2020), 103394.

[47] D. Terentyev, A. Bakaev, A. Serra, F. Pavia, K.L. Baker, N. Anento, Grain boundary mediated plasticity: the role of grain boundary atomic structure and thermal activation, Scr. Mater. 145 (2018) 1–4.
[48] D. Terentyev, X. He, A. Serra, J. Kuriplach, Structure and strength of ⟨110⟩ tilt grain boundaries in bcc Fe: an atomistic study, Comput. Mater. Sci. 49 (2) (2010) 419–429.
[49] M. Dewald, W.A. Curtin, Multiscale modeling of dislocation/grain-boundary interactions: III. 60 degrees dislocations impinging on Sigma 3, Sigma 9 and Sigma 11 tilt boundaries in Al, Model. Simul. Mater. Sci. Eng. 19 (5) (2011).
[50] W.S. Yu, Z.Q. Wang, Interactions between edge lattice dislocations and Sigma 11 symmetrical tilt grain boundaries in copper: a quasi-continuum method study, Acta Mater. 60 (13–14) (2012) 5010–5021.
[51] N. Miyazawa, S. Suzuki, M. Hakamada, M. Mabuchi, Atomic simulations of interactions between edge dislocations and a twist grain boundary in Mg, Mater. Trans. 61 (6) (2020) 1063–1069.
[52] A. Dubinko, C. Yin, D. Terentyev, A. Zinovev, M. Rieth, S. Antusch, M. Vilémová, J. Matějíček, T. Zhang, Plastic deformation in advanced tungsten-based alloys for fusion applications studied by mechanical testing and TEM, Int. J. Refract. Met. Hard Mater. 105409 (2020).
[53] E. Gaganidze, D. Rupp, J. Aktaa, Fracture behaviour of polycrystalline tungsten, J. Nucl. Mater. 446 (1–3) (2014) 240–245.
[54] F. Arbeiter, E. Diegele, U. Fischer, A. Garcia, A. Ibarra, J. Molla, F. Mota, A. Moslang, Y.F. Qiu, M. Serrano, F. Schwab, Planned material irradiation capabilities of IFMIF-DONES, Nucl. Mater. Energy 16 (2018) 245–248.